Adaptive molecular decomposition: Large-scale quantum chemistry for liquids

Tommi T. Järvi, Leonhard Mayrhofer, Jussi Polvi, Kai Nordlund, Lars Pastewka et al.

Additional information on J. Chem. Phys.

Adaptive molecular decomposition: Large-scale quantum chemistry for liquids

Tommi T. Järvi,[1,2] Leonhard Mayrhofer,[1] Jussi Polvi,[3] Kai Nordlund,[3] Lars Pastewka,[1,4,a] and Michael Moseler[1,5]

[1]*Fraunhofer Institute for Mechanics of Materials IWM, Wöhlerstrasse 11, D-79108 Freiburg, Germany*
[2]*Karlsruhe Institute of Technology, Institute of Applied Materials—Reliability of Components and Systems (IAM-ZBS), D-76131 Karlsruhe, Germany*
[3]*Department of Physics, University of Helsinki, P.O. Box 43, FI-00014 Helsinki, Finland*
[4]*Department of Physics and Astronomy, Johns Hopkins University, 3400 North Charles Street, Baltimore, Maryland 21218, USA*
[5]*Freiburger Materialforschungszentrum, Stefan-Meier-Str. 21, D-79104 Freiburg, Germany and Albert-Ludwigs Universität, Physikalisches Institut, Hermann-Herder-Str. 3, D-79104 Freiburg, Germany*

We present a linear-scaling method based on self-consistent charge non-orthogonal tight-binding. Linear scaling is achieved using a many-body expansion, which is adjusted dynamically to the instantaneous molecular configuration of a liquid. The method is capable of simulating liquids over large length and time scales, and also handles reactions correctly. Benchmarking on typical carbonate electrolytes used in Li-ion batteries displays excellent agreement with results from full tight-binding calculations. The decomposition slightly breaks the Hellmann-Feynman theorem, which is demonstrated by application to water. However, an additional correction also enables dynamical simulation in this case. © *2013 American Institute of Physics*. [http://dx.doi.org/10.1063/1.4793708]

I. INTRODUCTION

A wide range of methods are employed to predict and explain chemistry *in silico*, starting from non-reactive molecular mechanics force fields[1] through reactive potentials[2–4] all the way to first principles methods. A large part of chemistry occurs in the liquid phase, but liquids are also one of the most difficult systems to model because of their variable, dynamic structure. While non-reactive properties are adequately addressed by force fields, reactions pose a challenge. Many different elements are often present, making the development of *transferable* reactive potentials a difficult and time-consuming task. Additional complications arise for systems where electrostatic interactions and charge transfer are crucial.[5–7]

First principles methods, while transferable and easy to use for any elemental composition, do not scale linearly as system size increases. Unfortunately, the disordered nature of liquids often mandates the dynamical simulation of relatively large systems. With these challenges in mind, several linear-scaling methods for quantum mechanical calculations have been developed, each with its own advantages and drawbacks. These include general methods,[8–12] methods taking advantage of the structure of particular types of systems,[13–15] as well as methods relying on fitting potential energy surfaces to *ab initio* data.[16,17] For reviews of different methods, see, e.g., Refs. 18–22. No single method thus seems to have established itself as a first choice for a wide range of systems. As an alternative to full linear scaling methods, quantum mechanics/molecular mechanics (QM/MM) approaches for reactions within the liquid phase have been developed recently.[13,15,23] These approaches identify reactive sites and treat these quantum mechanically. However, they share some of the limitations of non-reactive force fields.

Between classical and quantum approaches, the tight-binding (TB) approximation[24–29] is an intermediate method that retains some of the transferability of *ab initio* methods by considering the electronic subsystem explicitly. Yet, it requires some parametrization. While TB is order of magnitude faster than real first principles methods, it scales similarly with system size.

In this work, we address the scaling problem by developing a linear-scaling tight-binding methodology. In contrast to traditional linear scaling schemes that exploit the fact that the multiplication of two sparse matrices takes linear time, our method starts from a block diagonal Hamiltonian, which can be straightforwardly solved in linear time, and then corrects for pair interactions. We follow an approach somewhat similar to QM/MM: We exploit the liquid substructure and treat intermolecular and intramolecular interactions separately. In contrast to present QM/MM approaches, all interactions are treated fully quantum mechanically in our model. Reactions are then naturally modeled by dynamically merging multiple molecules into a single "quantum" region. This avoids many of the artifacts that arise when converting a single molecule from a classical to a quantum description, such as a mismatch in chemical potentials.[15] In the final part of this paper we use our method to compute the solvation properties of lithium in ethylene and propylene carbonate.

a)Electronic mail: lars.pastewka@iwm.fraunhofer.de.

II. LINEAR-SCALING METHOD

As a basis for our method, we use self-consistent charge non-orthogonal tight-binding (SCC-NOTB),[24–27] as implemented in an in-house code. The basic method is covered extensively in Refs. [28] and [29]. Linear scaling is achieved by expanding into molecule pairs.[30] Formally, the system energy is expanded in *n*-body terms as in Refs. [30–32], with

$$E = \sum_{I=1}^{N} E^I + \sum_{I<J}^{N} V^{IJ} + \cdots, \tag{1}$$

where E^I is the energy of the isolated molecule I, and

$$V^{IJ} = E^{IJ} - E^I - E^J, \tag{2}$$

where E^{IJ} is the energy of a system composed of molecules I and J only. When using indices, we denote molecules by capital latin letters (I, J, K), atoms by lowercase letters (i, j, k), and orbitals by greek letters (μ, ν). We terminate the series at the molecule pair term. The decomposition then becomes linear scaling by nature, since pairs only contribute a non-negligible V^{IJ} if the respective molecules sit in each other's vicinity. Convergence of this type of series was investigated by, for instance, Dahlke *et al.*,[33] who found that for water hexamers, the error for the pairwise sum was around 1 kcal/mol ($\sim$40 meV), when electrostatic embedding was included.

Improving the convergence of the series in Eq. (1) indeed requires taking the electrostatic background of the liquid into account. The fact that the self-consistent charge tight-binding method incorporates Coulomb interactions between the atomic partial charges provides a natural way to accomplish this. Similar to Ref. [31], the charge self-consistency loop uses the energy to first-order molecular contributions (first sum of Eq. (1)) only. That is, the Hamiltonians of the molecular subsystems are solved independently of each other, except that each molecule feels the electrostatic potential from the others.

Simply solving the first-order contributions completely separately does not allow charge transfer between molecules. Thus, we keep the molecules otherwise decoupled, but determine orbital occupancies globally. This way, charge is allowed to flow unrestricted, which is important in describing, for example, the solvation of lithium in carbonates as discussed below.

For the molecule pairs, the total charge of the pair system is then taken as the sum of the constituent molecules' charges. We then carry out a non-self-consistent calculation, where the electrostatic potential obtained at first order is used. Here, it is assumed that the self-consistent charges in the pair calculation are very similar to those of the constituent molecules. Another reason to avoid a self-consistent charge (SCC) calculation for each pair is to ensure consistency against the molecular calculations subtracted in Eq. (2).

We will now cast the above method into the language of self-consistent charge density-functional tight-binding (SCC-NOTB). First, let H denote the full Hamiltonian and S the full overlap matrix of the atomistic system under consideration, both of which are assembled using the usual Slater-Koster transformation rules.[34] Then, the total energy of the system

is given by $E^{\text{tot}} = E + \frac{1}{2}\sum_{ij} V_{ij}^{\text{rep}}$ with

$$E = \sum_a f(\varepsilon_a)\langle a|H|a\rangle + \frac{1}{2}\sum_i \phi_i \delta q_i. \tag{3}$$

Here, $\phi_i = \sum_j \gamma_{ij}(R_{ij})\delta q_j$ is the effective electrostatic potential at atom i. Additionally, V_{ij}^{rep} is a repulsive pair contribution that has no influence on the electronic structure.

State $|a\rangle$ has eigenenergy ε_a and is populated according to the Fermi-Dirac occupation function $f(\epsilon)$. The charge fluctuations $\delta q_i = q_i - q_i^0$ are defined with respect to the Mulliken charges q_i, where q_i^0 is the Mulliken charge on the charge-neutral atom.[28,29,35] The Mulliken charges are given by

$$q_i = \frac{1}{2}\sum_a f(\varepsilon_a)\sum_{\mu\in i}\sum_{j\nu}(a_{i\mu}^* S_{i\mu j\nu}a_{j\nu} + a_{j\nu}^* S_{j\nu i\mu}a_{i\mu}), \tag{4}$$

where $a_{i\mu}$ denote the coefficients of $|a\rangle$ in the appropriate basis. The term $\gamma_{ij}(R_{ij})$ that determines the electrostatic potential ϕ_i then describes the strength of the electrostatic interaction and needs to approach the asymptotic behavior $\gamma_{ij}(R_{ij}) \to R_{ij}^{-1}$ for large distance R_{ij} of the atoms i and j. For small distances it depends on the shape of the charge.

The eigenstates $|a\rangle$ are obtained by minimizing the energy E with respect to all $|a\rangle$ subject to the orthonormality constraint $\langle a|S|b\rangle = \delta_{ab}$. This variational procedure leads to the one electron Schrödinger equation

$$(H^{\text{eff}}[|a\rangle] - \varepsilon_a S)|a\rangle = 0, \tag{5}$$

with the effective Hamiltonian H^{eff}. Its matrix elements $H_{i\mu j\nu}^{\text{eff}} = \langle i\mu|H^{\text{eff}}|j\nu\rangle$ are given by

$$H_{i\mu j\nu}^{\text{eff}}[|a\rangle] = H_{i\mu j\nu} + \frac{1}{2}S_{i\mu j\nu}(\phi_i[|a\rangle] + \phi_j[|a\rangle]), \tag{6}$$

and contain a band-structure contribution (first term) and a contribution that is due to electrostatics (second term). Note that in terms of the effective Hamiltonian the total energy becomes

$$E = \sum_a f(\varepsilon_a)\langle a|H^{\text{eff}}|a\rangle - \frac{1}{2}\sum_i \phi_i \delta q_i, \tag{7}$$

which has a structure identical to Eq. (3) but the second term has a minus sign. This is the double counting correction. Since the δq_k (and thus ϕ_k) depend on the eigenstates $|a\rangle$, Eq. (5) is nonlinear and needs to be solved self-consistently.

Let us now turn to the energy expansion of Eq. (1). Analogous to the energy, we decompose the total Hamiltonian H (and total overlap matrix S) into a block-diagonal Hamiltonian H^0 (and overlap matrix S^0) that describes noninteracting molecules. The Hamiltonian H^0 contains the molecular blocks on the diagonal of H, and can be decomposed into the Hamiltonians H^I that act in the subspace of each molecule such that $H^0 = \sum_I H^I$. Correspondingly, the set of eigenvectors of H^0 can be written as $\{|a^0\rangle\} = \cup_I\{|a^I\rangle\}$. In addition, we define pair Hamiltonians H^{IJ} (and overlap matrices S^{IJ}), which are sub-blocks that act in the subspace spanned by molecules I and J. This decomposition is illustrated in Fig. 1.
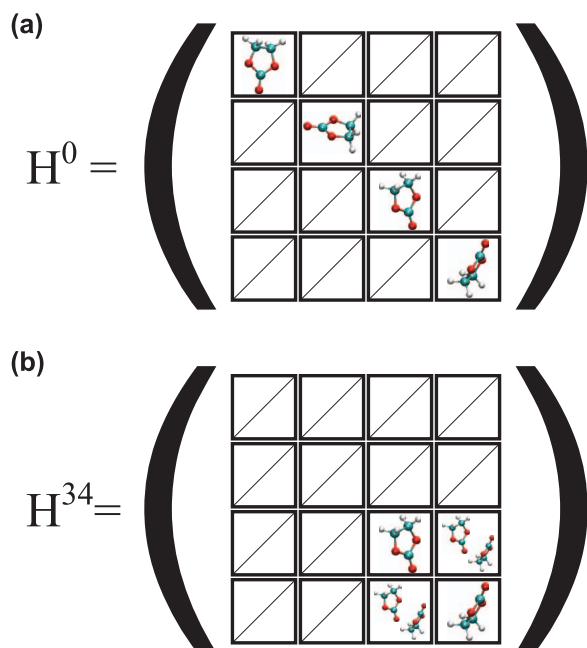
(a)

(b)

FIG. 1. Schematic illustration of the molecularly decomposed Hamiltonian matrices for four ethylene carbonate molecules. (a) The block diagonal form of the global Hamiltonian H^0 where all blocks without a picture of a molecule have zero entries. (b) The Hamiltonian H^{IJ} that determines the interaction between molecules 3 and 4 in this picture. The diagonal terms are identical to the diagonal terms of H^0 for molecules 3 and 4, but H^{34} additionally contains the matrix elements that govern the intermolecular interaction.

With these definitions we first solve the decomposed system for each molecule I in analogy to Eq. (5) as

$$(H^{I,\text{eff}}[|a^0\rangle] - \varepsilon_{a^I} S^I)|a^I\rangle = 0, \qquad (8)$$

where we highlight the fact that the minimization is carried out self-consistently, since the electrostatic potential (see Eq. (6)) varies from iteration to iteration. Each molecule's effective Hamiltonian depends on all the others in that the electrostatic potential ultimately depends on the combined eigenstates $|a^0\rangle$. Note also that the occupation function (f in Eq. (4)) is the same function for all molecules, denoted f^0, with a common Fermi energy. As stated above, occupancies are determined globally to allow charge transfer between the molecules.

Once the decomposed system is solved, we then solve the Hamiltonian for each pair I-J as

$$(H^{IJ,\text{eff}}[|a^0\rangle] - \varepsilon_{b^{IJ}} S^{IJ})|b^{IJ}\rangle = 0. \qquad (9)$$

One of the keys to our method is the definition of the electrostatic potential ϕ_i that enters Eqs. (8) and (9). We define this to be given by the decomposed eigenstates $|a^0\rangle$ only. It thus acts as the electrostatic embedding term for the molecule pairs.

In the pair calculation, we adjust the local Fermi-level for the pair IJ such that its total charge Q_{IJ} is identical to the sum of the Mulliken charges Q_I and Q_J of molecules I and J, respectively. In terms of the occupation functions f^0 and f^{IJ}, this condition becomes

$$\sum_{b^{IJ}} f^{IJ}(\varepsilon_{b^{IJ}}) = \sum_{a^I} f^0(\varepsilon_{a^I}) + \sum_{a^J} f^0(\varepsilon_{a^J}). \qquad (10)$$

The secular equation (9) is then solved only once, since the eigenstates $|b^{IJ}\rangle$ do not enter the effective Hamiltonian $H^{IJ,\text{eff}}$. This scheme corresponds to going to second order in series (1) for the orbital interactions while evaluating the SCC loop at first order only.

Putting the above decomposition in terms of expansion (1), we have

$$E = \sum_I E^I + \sum_{I<J} V^{IJ} + \frac{1}{2}\sum_i \phi_i \delta q_i \qquad (11)$$

with $V^{IJ} = E^{IJ} - E^I - E^J$, and

$$E^I = \sum_{a^I} f^0(\varepsilon_{a^I})\langle a^I|H^I|a^I\rangle \quad \text{and}$$

$$E^{IJ} = \sum_{b^{IJ}} f^{IJ}(\varepsilon_{b^{IJ}})\langle b^{IJ}|H^{IJ}|b^{IJ}\rangle. \qquad (12)$$

In order to carry out molecular dynamics simulation, we require forces which are the derivatives of the total energy, Eq. (11), with respect to the positions. As the sum over the molecular terms corresponds to a single self-consistent tight-binding calculation with a block-diagonal Hamiltonian, it satisfies the Hellmann-Feynman theorem. However, the $H^{IJ,\text{eff}}$ in Eq. (9) depend on the eigenstates at first order, i.e., on $|a^I\rangle$ through the electrostatic potential due to the Mulliken charges. Thus, the $|b^{IJ}\rangle$ are no longer exact eigenstates of H^{IJ} on the second line of Eq. (12). A correction is, however, difficult to evaluate, and we therefore neglect the issue in the following treatment. This leads to breaking the Hellmann-Feynman theorem, which may cause energy conservation problems. We will discuss and evaluate the magnitude of these in the specific application examples below. Note that this problem only affects SCC calculations. Without self-consistent charges, energy is conserved by construction.

Similar methods have been previously used with *ab initio* theory.[32,36] However, in these works the molecular structure of the system was assumed to stay unchanged during the simulation. This approximation obviously requires the molecular structure to be given initially, and it furthermore breaks down as soon as reactions occur.

In order to allow for reactions, we decompose the system into its molecular constituents at each time step. This is similar in spirit to the method employed by Yamaguchi *et al.*[37] for gas-phase carbon. However, decomposition based solely on a geometric cutoff criterion would potentially cause problems in a liquid because such an approach ignores the liquid's actual binding structure. To properly estimate the strength of the interaction between two molecules, we would need to compute the maximum covalent bond energy[38] between each molecule pair at each time step. This requires solution of all potential pairs and is computationally intensive. Instead, we take an intermediate approach and use the Hamiltonian matrix to determine whether two atoms belong to the same molecule: A cutoff is imposed on the maximum absolute value of the matrix elements corresponding to the interaction between the two molecules. This way it is the strength of the interaction which determines the decomposition. For increased efficiency, the analysis is always started from the molecular

structure of the previous time step. Then, molecules are joined and separated according to the chosen cutoff.

In detail, the decomposition algorithm is as follows. At each time step, the molecular structure from the previous time step is used as a starting point. Then, we first attempt to separate each existing molecule into smaller subunits. For this, we use an algorithm based on single-linkage hierarchical clustering.[39] The details of the algorithm are

For each molecule I:

1. Initialize each atom in the molecule to its own single-atom subunit.
2. Set $n = 0$ and loop over atom pairs i-j, with i and j in different subunits within the molecule:
   If $(\max_{\mu\nu}\{|H_{i\mu j\nu}|\} > \text{cutoff}) \Rightarrow$
      Join the subunits to which atoms i and j belong to a single subunit
      Increment n
3. If $(n > 0) \rightarrow 2$.
4. Split molecule if more than a single subunit is left

After this, we check if any previously separate molecules need to be joined. Looping over molecule pairs I-J, two molecules are joined, if $\max_{\mu\nu}\{|H_{i\mu j\nu}|\} > \text{cutoff}$ for any $i \in I$, $j \in J$. At the beginning of the simulation, all atoms are placed in a single molecule. This dynamic decomposition during a molecular dynamics run is linear-scaling in the number of molecules, since separation acts on molecules and joining can be implemented using the usual linked-cell algorithm.[40]

The scaling of the method is illustrated in Fig. 2, which shows the total simulation time and the time spent solving the secular equations for the full and decomposed cases. Overall, no single factor was found to dominate the execution time in the decomposed case, displaying balanced performance. Note that while the decomposition is linear-scaling, other parts of the simulation such as the particle-mesh Ewald method, which scales as $\mathcal{O}(N \log(N))$, are not.

To illustrate the decomposition in a simple model system, we take the water dimer. Specifically, we use the
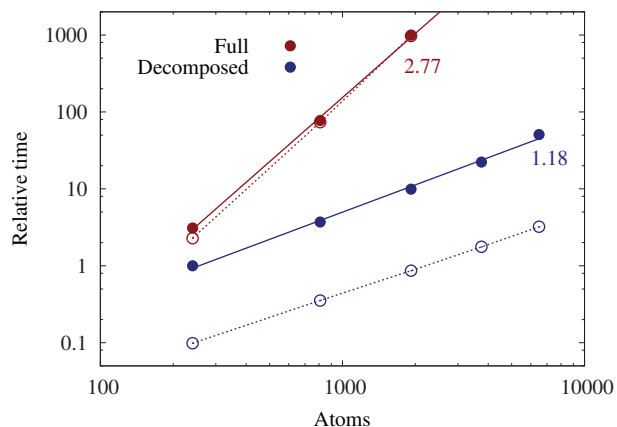

FIG. 2. Scaling of the molecular decomposed method compared to full tight-binding calculations. A short simulation was run for periodic cells of liquid water. The execution time for the decomposed method with 240 atoms has been normalized to unity. Fitted scaling exponents are shown next to the lines and the open symbols show the time required for diagonalization.
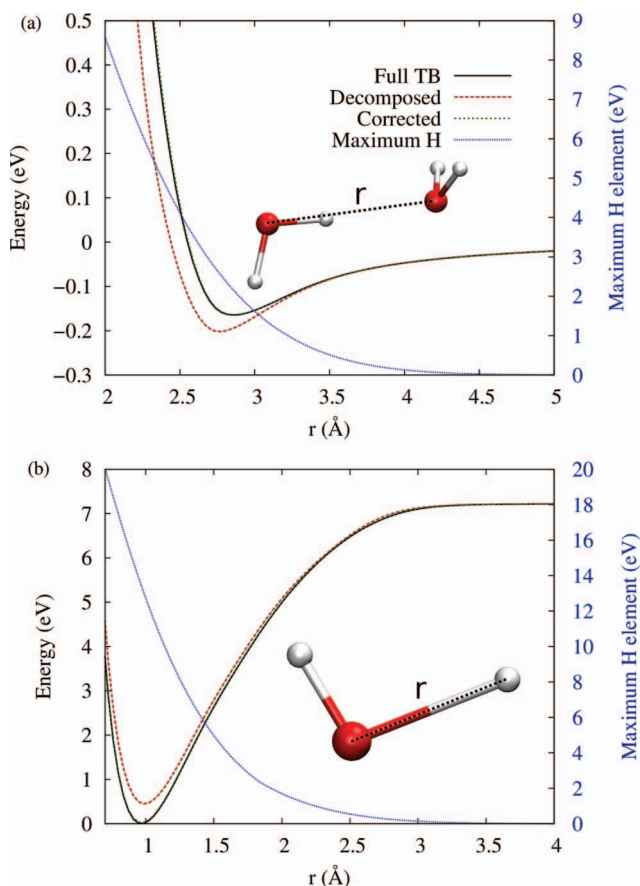

FIG. 3. Decomposition for (a) the intermolecular interaction in a water dimer and (b) for the O–H bond in a water molecule. The right axes show the maximum Hamiltonian matrix element between the subunits. When this decreases below 1–2 eV for the water dimer (around 3 Å), the error in the decomposition becomes negligible. Both panels also show the decomposed result with the correction introduced in Sec. III. The curves barely differ from those of the full calculation.

density-functional based *mio-0-1* parametrization,[41] (SCC-DFTB).[28,42] The upper panel in Figure 3 illustrates the difference between the decomposed and the full tight-binding solutions when the distance between the two water molecules in the dimer is changed. For the decomposed case, we keep the two molecules decomposed manually along the full trajectory. Because only two molecules are involved, the error comes from the different Mulliken charges at first order in the expansion as compared to the ones from a full treatment. Note that for a non-SCC calculation, the solutions match exactly (not shown). Because of the nature of the hydrogen bond, the water dimer is a worst case scenario and in most cases the error is significantly smaller (see Sec. III). Even here, as the intermolecular elements of the Hamiltonian matrix decrease below 1–2 eV, the decomposed solution no longer deviates much from full tight-binding. Note, however, that there is still significant interaction between the molecules at this point.

Next, we investigate the breaking of a covalent bond. The lower panel in Fig. 3 shows the dissociation of a water molecule by stretching of the O–H bond. Again, we manually keep the H_2O decomposed into an OH and a H fragment during the whole trajectory. With increasing bond length the relative error quickly becomes small and is about 2% at 2 Å. Note

that we here break a covalent bond to show that the method applies equally well for reactive simulations. In a full simulation, the OH and H would be merged into a single molecule hence following the energy given by the full tight-binding solution in the lower panel of Fig. 3.

This linear-scaling scheme is of course restricted to systems such as liquids, which can be decomposed into weakly interacting subsystems. The advantage, on the other hand, is that the prefactor is small, such that significant speedups are already obtained at very small system sizes. Also, note that as shown by the water molecule in Fig. 3, the decomposition of covalently bonded systems is possible, although it misestimates binding energies by about 10%. This approach is known as the fragment molecular orbital method.[43]

III. DYNAMICS

Previous studies that used similar many-body expansions discussed exclusively static properties.[30–32] Convergence of energetics was addressed without regard to dynamic simulations, which in addition to energies require accurate forces for energy conservation. As pointed out above, the many-body expansion indeed causes problems when calculating forces. As we will show here, the severity of the problems varies case by case. In carbonate electrolytes the breaking of the Hellmann-Feynman theorems turns out to be negligible, while in water it is not. However, we demonstrate a correction with which dynamical simulation is also possible for water.

We test the method in two liquids. Propylene carbonate, depicted in Fig. 4 is a typical component in lithium-ion battery electrolytes. While liquid at room temperature, it does not contain strong specific intermolecular bonds. The other example, water, forms a relatively strong network of hydrogen bonds.

Let us first examine the decomposition in the case of propylene carbonate (PC), where there is relatively weak bonding between the molecules and energy conservation is nearly perfect. In the production runs for ethylene and propylene carbonate below, we used a cutoff of 2 eV for the decomposition. This value gives a decomposition, where the average number of subunits in a simulation at 400 K is on average roughly 90% of the number of carbonate molecules in the cell. The number of subunits in a 1 ps run is shown in Fig. 5 along with the partial charge on a carbonyl oxygen and the force on the respective PC molecule in a short trajectory.

FIG. 5. (a) Number of decomposed subunits in a simulation with 125 PC molecules. (b) Partial charge of an arbitrary carbonyl oxygen in a full calculation and using the decomposition. (c) Total force on the PC molecule containing that oxygen atom.

FIG. 4. Ethylene carbonate (EC) and propylene carbonate (PC).

Here, the errors in both charge and force are negligible and the maximum error in the force reaches about 0.06 eV/Å. The maximum errors in the force for the Hamiltonian and electrostatic components are ∼0.06 and 0.02 eV/Å, respectively. The maximum error in energy for the Hamiltonian contribution is about 0.01%, while that for the electrostatic interaction is roughly 2%. No excessive thermalization is required as the temperature in an NVE simulation at 400 K rises roughly only by 1 K/ps.

Next, let us turn to water. Here, we find that in an NVE simulation the breaking of the Hellmann-Feynman theorem results in significant mismatch of forces and energies and

hence heat production. With a Berendsen thermostat,[44] it is possible to constrain the temperature rise to around 10 K (at 300 K) with a relaxation time constant of 100 fs. We used an energy cutoff of 6 eV in the Hamiltonian matrix elements. At this cutoff, the decomposition is such that each water molecule has its own quantum zone and no two water molecules are joined. Figure 6 shows the partial charge on an oxygen atom in one of the water molecules and the total force on the molecule containing that oxygen. Although the average value of the charge is roughly correct, the fluctuations are suppressed in the decomposed case. Correspondingly the error in the force, shown in the lower panel of Fig. 6, is large and reaches a maximum of ∼0.4 eV/Å. The large error is attributable to the strong bonding between water molecules. We neglect this bonding in the computation of the charges from the fully decomposed Hamiltonian. Thus, two water molecules cannot hybridize in the charge self-consistency loop. This leads to a suppression of the transfer of charge between water molecules. Each water is charge neutral in the decomposed simulations while we observe charges of the order of 0.05|e| per water molecule in the full tight-binding calculations. This is the origin of the large error in the charge per atom and consequently also the forces shown in Fig. 6.

In order to correct this problem, a full variational solution of expansion (1) would be necessary. However, to alleviate the problem, we propose the following first-order correction, which we apply to the *Coulomb interaction only*. In terms of expansion (11), we apply a correction to the third term. Instead of the Mulliken charges derived from the first-order eigenstates $|a^I\rangle$, we base the Coulomb interaction on a weighted average of the charges derived from the (non-self-consistent) pair calculation. Thus, we take

$$q_i = \frac{\sum_J q_i^{IJ} w^{IJ}}{\sum_J w^{IJ}}, \tag{13}$$

where q_i^{IJ} is the charge of atom i derived from the eigenstates $|b^{IJ}\rangle$ for the pair I–J. If molecule I is not interacting with other molecules, we leave the charge unchanged. Here, w^{IJ} is the corresponding weight for the pair, for which we choose $(\max_{\mu\nu}\{|H_{i\mu j\nu}|\})^2$, where $i \in I$ and $j \in J$. With this choice, the contribution from non-interacting molecule pairs vanishes, while a single strongly interacting pair will dominate the charges. As the above expression potentially changes the total charge, we additionally correct all charges by adding a (small) constant to ensure the total charge is preserved.

Figure 3 shows the water dimer interaction energy using the above scheme, with the corrected curve coinciding with full TB almost exactly. The difference comes from the non-self-consistent nature of the pair calculation. Similarly, the error in the Mulliken charge for the dynamical simulation shown in Fig. 6 is greatly reduced. The effect on the error in the force is not as pronounced. However, the simulation becomes much more stable. In an NVE simulation including the correction, temperature rises by ∼4 K/ps, which, although more than in the case of PC, allows dynamical simulation using only a weak thermostat. Finally, note that in cases where the charges stay almost unchanged in the decomposition, such
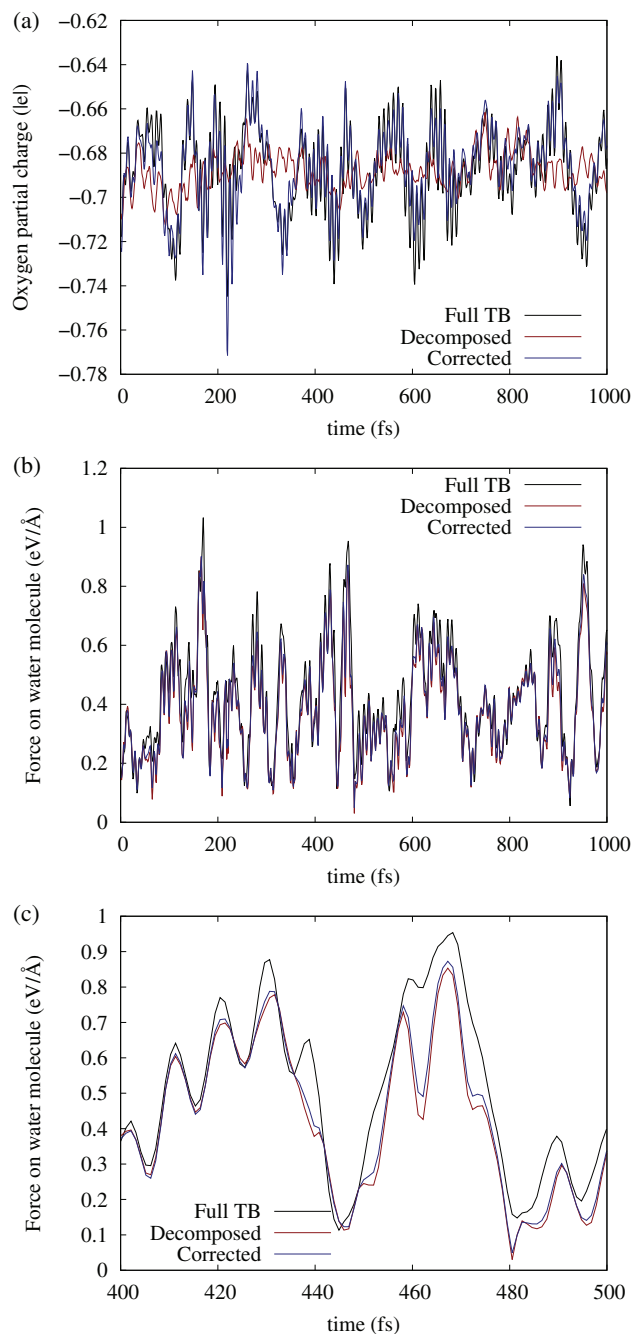
FIG. 6. (a) Partial charge of an arbitrary oxygen atom in water in a full calculation and using the decomposition. (b) Total force on the water molecule containing that oxygen atom. (c) Detailed view of a part of the curve in the middle panel. All panels additionally show the effect of the correction described in Sec. III.

as with PC here, the corrected scheme is equivalent to the original expansion.

IV. SOLVATION OF LITHIUM IN CARBONATE ELECTROLYTES

To illustrate the power of the method, we employ it to benchmark tight-binding for studying the solvation of lithium in carbonate electrolytes, namely, ethylene and propylene carbonate which are depicted in Fig. 4.

TABLE I. Simulation cells used for modelling the electrolytes.

	Molecules	Density (g/cm^3)	
		310 K	400 K
EC	125	1.3201	1.2174
PC	125	1.2279	1.1255

An additional component is necessary to model the electrolytes and their interaction with lithium. As no density-functional tight-binding (DFTB) parametrization including lithium is currently available, we develop interaction models for Li-{C, H, O}. Fortunately, due to the fact that lithium assumes the ionic state Li$^+$ with a partial charge very close to $+1|e|$ in all configurations relevant to the present study, the interactions are mainly Coulombic. In Appendix A, we thus parametrize Lennard-Jones pair potentials for the interactions. The pair-potential acts in addition to the electrostatic interaction where the lithium is modeled by a point charge of magnitude $+1|e|$.

In order to supply reasonable starting configurations for TB, simulation cells containing the electrolyte are relaxed using classical molecular dynamics (MD). More details are given in Appendix B.

A. Simulation procedure

Here, we concentrate on the coordination of lithium with electrolyte molecules at the limit of low salt concentration. First, electrolyte systems consisting of 125 molecules were created and relaxed using classical force fields as explained in Appendix B. This equilibrates the liquid structure and volume. The volume was then held fixed during the tight-binding simulations. The parameters of the simulation cells are summarized in Table I.

After relaxing the cells, we searched for free space in the form of spheres of about 3 Å radius. Ten of these were selected at random for the introduction of a lithium ion. This gives ten different systems with one lithium ion per cell for both ethylene carbonate (EC) and PC. The positive lithium charge was compensated by a negative jellium background. For the electrostatic interaction we used the particle mesh

Ewald method[45, 46] with a real-space cutoff of 1.0 nm and a 32^3 grid that results in a grid spacing of roughly 0.8 Å. The exact grid spacing depended on the cell size. We use a time step of 1 fs. Each system was then relaxed and equilibrated at 400 K for 20 ps. This temperature was chosen to ensure the liquid phase for pure EC.

B. Lithium solvation

Solvation of lithium in PC was recently studied in detail by Kameda *et al.*[47] using neutron diffraction. The first solvation shell was found to consist on average of 4.5 PC molecules, with an average Li–O bond length of 2.04 Å and Li–O–C angle of 138°. Several experiments have used infrared and Raman spectroscopy to look at the solvation of various salts and solvents, with the consensus being that lithium is surrounded predominantly by 4 carbonate molecules.[48–54] However, it also seems that 5- and even 6-coordinated configurations are present.[48, 52, 55] On the other hand, also significantly lower numbers have been reported,[49, 56–58] and it seems that at high salt concentration, configurations where lithium is sandwiched between two carbonates are possible.[49, 56]

The solvation of lithium has also been modelled extensively. Using classical force fields, Borodin and Smith[59] reported a solvation shell of on average 3.6 EC molecules around Li at room temperature, whereas *ab initio* molecular dynamics results point to a value of 4.[60–62]

From the present simulations, averaging over the latter half of the 20 ps equilibration runs, a solvation shell of 4.8 was obtained for PC at 400 K. Simulations using EC and simulations at a lower temperature gave very similar results. The average Li–O–C and O–Li–O angles were 143° and 106°, respectively. The observed lithium solvation shell fits very well with the experimental estimate of 4–5 molecules. The average Li–O–C angle compares well to the neutron diffraction result of 138° of Ref. 47. The average O–Li–O angle agrees well with the value of ∼110° from *ab initio* molecular dynamics (AIMD).[61]

The angular distributions for PC are shown in Fig. 7. The results for EC are similar. The distributions of Li–O–C agree well with Ref. 61. In contrast, the O–Li–O distributions have a different shape: Instead of simply centering around ∼110°,
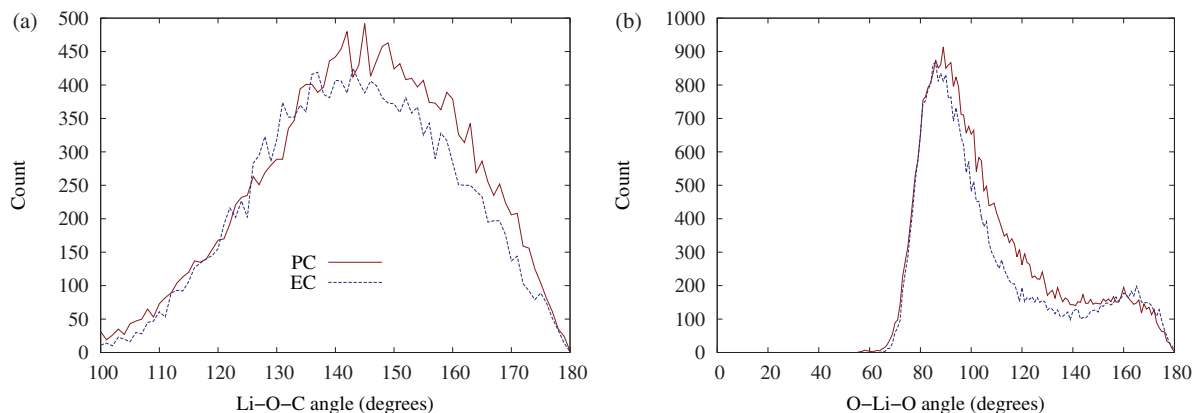

FIG. 7. Angular distributions for Li solvated in EC and PC at 400 K.

TABLE II. Lennard-Jones parameters for lithium-electrolyte molecule interactions.

	ϵ (eV)	σ (Å)
Li–O	0.02	2.2
Li–C	0.05	2.3
Li–H	0.01	1.9

there is a major peak around 90° with a tail towards 180°. Indeed, it seems that in our simulations Li prefers solvation in a partly filled six-coordinated shell. There is no experimental result on the shape of the O–Li–O angle distribution. We can only state that as far as the number of molecules in the solvation shell and the average Li–O–C angle our results agree with the experimental results to similar accuracy as those of AIMD simulations.[61]

V. CONCLUSIONS

We presented a method that dynamically decomposes a liquid system into its constituents and employs that decomposition to efficiently solve for the electronic structure in a tight-binding model. This allows linear scaling of computation time with system size. In principle, this scheme could also be used to obtain the decomposition dynamically as part of a more accurate method such as density functional theory (DFT). While the strong intermolecular interactions in water pose a challenge to the method, dynamical simulation is possible with an additional correction to the Mulliken charges of the decomposed system. The usefulness of the method was demonstrated in simulations of carbonate electrolytes. All these simulations were carried out on a single CPU. Since the prefactor is small, the method can be used for quantum calculations with millions of atoms on currently available computing hardware.

ACKNOWLEDGMENTS

APPENDIX A: LITHIUM-ELECTROLYTE INTERACTION

Lithium is in the singly charged state, Li^+, in all configurations relevant to this study. The interaction between lithium and other species is thus predominantly Coulombic, and can be accurately described by an electrostatic interaction of the singly charged Li-ion combined with a L-J potential, which provides the necessary repulsion. Fitting of the interaction components is described in the following, and the resulting parameters summarized in Table II.

Note that while this approach is sufficient for the present study where only interactions of isolated lithium with the electrolyte are important, a full tight-binding parametrization needs to be developed to model Li-metal electrodes or other systems where the Li-Li interaction becomes significant.

Reference energies for the fit were computed using DFT. These calculations were performed using the SIESTA code,[9] version 3.1. Exchange and correlation were described within the spin-polarized generalized gradient approximation as implemented by Perdew, Burke, and Ernzerhof.[63] The effects of the core electrons were taken into account by the use of norm-conserving pseudo-potentials[64–67] and a double zeta plus polarization (DZP) basis is employed for the wavefunction expansion. The radial cutoff of the basis orbitals is determined by an energy shift[9] of 0.02 eV in the radial part of the pseudo-atom Schrödinger equation. The spacing of the real-space integration grid is determined by a mesh cutoff energy of 1400 eV. As all systems were non-periodic, only Γ-point calculations were made.

1. Li–O

Lithium binds strongly to oxygen because of oxygen's strong electronegativity. Thus, the Li–O parametrization is by far the most important one.

The Li–O interaction was fit to Li^+-EC complexes, as these are a representative case of the bonding patterns observed in electrolytes. This system and all following systems containing Li^+ were embedded in vacuum and positively charged. We used two structures as reference, lithium coordinated to either one or four EC molecules. In the latter case, the complex assumes a tetrahedral configuration.[68] Table III shows the energy required to remove a single EC molecule from the complexes as well as the Li–O bond length. A very good correspondence between the DFT results and the potential is obtained, due to the simple Coulombic nature of the interaction.

2. Li–C

The lithium-carbon interaction was fit to the interaction between Li^+ and a hydrogen-terminated graphene flake (with

TABLE III. Reaction energies for removing EC from Li-EC complexes and bond lengths for Li–O bonds in the higher coordinated (reactant) complex. The cases marked with an asterisk were used in fitting the potential.

	Potential		DFT (present work)		DFT (Ref. 68)	
	ΔE (eV)	$r_{\text{Li-O}}$ (Å)	ΔE (eV)	$r_{\text{Li-O}}$ (Å)	ΔE (eV)	$r_{\text{Li-O}}$ (Å)
* Li^+-EC $\rightarrow Li^+$ + EC	1.99	1.91	1.91	1.82	2.20	1.76
* Li^+-(EC)$_4$ $\rightarrow Li^+$-(EC)$_3$ + EC	0.80	1.99	0.63	1.98	0.60	1.97
Li^+-(EC)$_5$ $\rightarrow Li^+$-(EC)$_4$ + EC	0.54	2.03	0.37	2.1	0.25	2.09

54 carbon atoms). The resulting binding energy and distance (1.73 eV and 2.39 Å) compared well to DFT values (1.76 eV, 2.37 Å). Additionally, we tested a different case where a Li-ion was substituted in place of a hydrogen in an ethane molecule. The lithium-carbon bond length from our potential was 2.27 Å, to be compared to 2.34 Å from DFT. The bond dissociation energy was equally well reproduced, with 0.67 and 0.76 eV for the potential and DFT, respectively.

3. Li–H

Parametrizing the lithium-hydrogen interaction from complexes involving electrolyte molecules was found difficult, because Li was found not to bind to the hydrogens in EC. The interaction between lithium and hydrogen is thus expected to be repulsive, as both are most often positively charged. In order to determine the LJ parameters, we fit the onset of the repulsive interaction in a LiH^+ dimer. A shallow L-J attractive well was chosen, so that any attraction in the simulations will be purely electrostatic.

APPENDIX B: MOLECULAR DYNAMICS WITH NON-REACTIVE FORCE FIELDS

To get properly relaxed input systems for tight-binding, molecular dynamics simulations were performed with the GROMACS simulation package[69] using the OPLS-AA all-atom force field.[70]

The OPLS parameters for EC and PC molecules were taken from recent work by Silva and Freitas.[71] The partial charges used were the MP2 charges shown in Table IV of Ref. 71 and the torsional parameters for the methyl group in propylene carbonate were taken from related types of interactions in the OPLS force field.[70]

The simulation protocol for each system included three phases. First, the systems were pre-relaxed at 300 K for 100 ps to remove the arbitrary order present in the hand-built initial configuration, after which a 0.5 ns NPT simulation at 1 bar was run. Each system was relaxed to 400 K using the V-rescale thermostat[72] with a time constant of 0.3 ps and a Parrinello-Rahman barostat[73] with a time constant of 1.0 ps for pressure coupling. Subsequently, a 2 ns stochastic MD simulation using Langevin dynamics[74] was run to make sure the liquid structure was properly equilibrated.

[1] A. R. Leach, *Molecular Modelling: Principles and Applications*, 2nd ed. (Prentice-Hall, Harlow, England, 2001).

[2] M. S. Daw and M. I. Baskes, "Embedded-atom method: Derivation and application to impurities, surfaces, and other defects in metals," Phys. Rev. B **29**, 6443 (1984).

[3] J. Tersoff, "New empirical approach for the structure and energy of covalent systems," Phys. Rev. B **37**, 6991 (1988).

[4] D. W. Brenner, "The art and science of an analytic potential," Phys. Status Solidi B **217**, 23 (2000).

[5] R. A. Nistor, J. G. Polihronov, M. H. Müser, and N. J. Mosey, "A generalization of the charge equilibration method for nonmetallic materials," J. Chem. Phys. **125**, 094108 (2006).

[6] P. T. Mikulski, T. Knippenberg, and J. A. Harrison, "Merging bond-order potentials with charge equilibration," J. Chem. Phys. **131**, 241105 (2009).

[7] L. Pastewka, T. T. Järvi, L. Mayrhofer, and M. Moseler, "Charge-transfer model for carbonaceous electrodes in polar environments," Phys. Rev. B **83**, 165418 (2011).

[8] N. Bernstein, "Linear scaling nonorthogonal tight-binding molecular dynamics for nonperiodic systems," EPL **55**, 52 (2001).

[9] J. M. Soler, E. Artacho, J. D. Gale, A. García, J. Junquera, P. Ordejón, and D. Sánchez-Portal, "The SIESTA method for *ab initio* order-N materials simulation," J. Phys.: Condens. Matter **14**, 2745 (2002).

[10] R. Zeller, "Towards a linear-scaling algorithm for electronic structure calculations with the tight-binding Korringa-Kohn-Rostoker green function method," J. Phys.: Condens. Matter **20**, 294215 (2008).

[11] M. J. Rayson and P. R. Briddon, "Highly efficient method for Kohn-Sham density functional calculations of 500–10 000 atom systems," Phys. Rev. B **80**, 205104 (2009).

[12] J. D. Goodpaster, T. A. Barnes, and T. F. Miller III, "Embedded density functional theory for covalently bonded and strongly interacting subsystems," J. Chem. Phys. **134**, 164108 (2011).

[13] R. E. Bulo, B. Ensing, J. Sikkema, and L. Visscher, "Toward a practical method for adaptive QM/MM simulations," J. Chem. Theory Comput. **5**, 2212 (2009).

[14] K. Varga, "Multidomain decomposition approach to large-scale electronic structure calculations," Phys. Rev. B **81**, 045109 (2010).

[15] N. Bernstein, C. Várnai, I. Solt, S. A. Winfield, M. C. Payne, I. Simon, M. Fuxreiter, and G. Csányi, "QM/MM simulation of liquid water with an adaptive quantum region," Phys. Chem. Chem. Phys. **14**, 646 (2012).

[16] Y. Wang, X. Huang, B. C. Shepler, B. J. Braams, and J. M. Bowman, "Flexible, *ab initio* potential, and dipole moment surfaces for water. I. Tests and applications for clusters up to the 22-mer," J. Chem. Phys. **134**, 094509 (2011).

[17] V. Babin, G. R. Medders, and F. Paesani, "Toward a universal water model: First principles simulations from the dimer to the liquid phase," J. Chem. Phys. Lett. **3**, 3765 (2012).

[18] D. R. Bowler, M. Aoki, C. M. Goringe, A. P. Horsfield, and D. G. Pettifor, "A comparison of linear scaling tight-binding methods," Model. Simul. Mater. Sci. Eng. **5**, 199 (1997).

[19] S. Goedecker, "Linear scaling electronic structure methods," Rev. Mod. Phys. **71**, 1085 (1999).

[20] S. Goedecker and G. E. Scuseria, "Linear scaling electrostructure methods in chemistry and physics," Comput. Sci. Eng. **5**(4), 14 (2003).

[21] K. Szalewicz, C. Leforestier, and A. van der Avoird, "Towards the complete understanding of water by a first-principles computational approach," Chem. Phys. Lett. **482**, 1 (2009).

[22] E. Rudberg and E. H. Rubensson, "Assessment of density matrix methods for linear scaling electronic structure calculations," J. Phys.: Condens. Matter **23**, 075502 (2011).

[23] A. Warshel and M. Lewitt, "Theoretical studies of enzymic reactions: Dielectric, electrostatic and steric stabilization of the carbonium ion in the reaction of lysozyme," J. Mol. Biol. **103**, 227 (1976).

[24] R. C. Kittler and L. M. Falicov, "Band theory for order-disorder phase transformations: CuAu," Phys. Rev. B **18**, 2506 (1978).

[25] M. O. Robbins and L. M. Falicov, "Electronic theory of ordering and segregation in transition-metal alloys," Phys. Rev. B **29**, 1333 (1984).

[26] W. A. Harrison, "Coulomb interactions in semiconductors and insulators," Phys. Rev. B **31**, 2121 (1985).

[27] F. Bechstedt, D. Reichardt, and R. Enderlein, "Self-consistent tight-binding method for total energy calculations of tetrahedral semiconductors including surfaces and defects," Phys. Status Solidi B **131**, 643 (1985).

[28] M. Elstner, D. Porezag, G. Jungnickel, J. Elsner, M. Haugk, T. Frauenheim, S. Suhai, and G. Seifert, "Self-consistent-charge density-functional tight-binding method for simulations of complex materials properties," Phys. Rev. B **58**, 7260 (1998).

[29] P. Koskinen and V. Mäkinen, "Density-functional tight-binding for beginners," Comput. Mater. Sci. **47**, 237 (2009).

[30] D. Hankins, J. W. Moskowitz, and F. H. Stillinger, "Water molecule interactions," J. Chem. Phys. **53**, 4544 (1970).

[31] K. Kitaura, T. Sawai, T. Asada, T. Nakano, and M. Uebayasi, "Pair interaction molecular orbital method: An approximate computational method for molecular interactions," Chem. Phys. Lett. **312**, 319 (1999).

[32] G. J. O. Beran, "Approximating quantum many-body intermolecular interactions in molecular clusters using classical polarizable force fields," J. Chem. Phys. **130**, 164115 (2009).

[33] E. E. Dahlke, H. R. Leverentz, and D. G. Truhlar, "Evaluation of the electrostatically embedded many-body expansion and the electrostatically embedded many-body expansion of the correlation energy by application to low-lying water hexamers," J. Chem. Theory Comput. **4**, 33 (2008).

[34] J. C. Slater and G. F. Koster, "Simplified LCAO method for the periodic potential problem," Phys. Rev. **94**, 1498 (1954).

[35] R. S. Mulliken, "Electronic population analysis on LCAO-MO molecular wave functions," J. Chem. Phys. **23**, 1833 (1955).

[36] S. S. Xantheas, "*Ab initio* studies of cyclic water clusters $(h_2o)_n$, $n = 1 − 6$. II. Analysis of many-body interactions," J. Chem. Phys. **100**, 7523 (1994).

[37] Y. Yamaguchi, L. Colombo, P. Piseri, L. Ravagnan, and P. Milani, "Growth of $sp-sp^2$ nanostructures in a carbon plasma," Phys. Rev. B **76**, 134119 (2007).

[38] N. Börsen, B. Meyer, O. Grotheer, and M. Fähnle, "e_{cov}—A new tool for the analysis of electronic structure data in a chemical language," J. Phys.: Condens. Matter **11**, L287 (1999).

[39] T. Hastie, R. Tibshirani, and J. Friedman, *The Elements of Statistical Learning*, 2nd ed. (Springer, 2009).

[40] M. P. Allen and D. J. Tildesley, *Computer Simulation of Liquids* (Oxford University Press, Oxford, England, 1987).

[41] However, we employ Gaussian[29] as opposed to the Slater-type[28] densities for the excess charges. This leads to energy differences of the order of $\lesssim 10$ meV.

[42] See http://www.dftb.org for the *mio-0-1* tight-binding parameter set.

[43] K. Kitaura, E. Ikeo, T. Asada, T. Nakano, and M. Uebayasi, "Fragment molecular orbital method: An approximate computational method for large molecules," Chem. Phys. Lett. **313**, 701 (1999).

[44] H. J. C. Berendsen, J. P. M. Postma, W. F. van Gunsteren, and J. R. Haak, "Molecular dynamics with coupling to an external bath," J. Chem. Phys. **81**, 3684 (1984).

[45] T. Darden, D. York, and L. Pedersen, "Particle mesh Ewald: An $N \cdot \log(N)$ method for Ewald sums in large systems," J. Chem. Phys. **98**, 10089 (1993).

[46] U. Essman, L. Perera, M. L. Berkowitz, T. Darden, H. Lee, and L. G. Pedersen, "A smooth particle mesh Ewald method," J. Chem. Phys. **103**, 8577 (1995).

[47] Y. Kameda, Y. Umebayashi, M. Takeuchi, M. A. Wahab, S. Fukuda, S. Ishiguro, M. Sasaki, Y. Amo, and T. Usuki, "Solvation structure of Li^+ in concentrated $LiPF_6$-propylene carbonate solutions," J. Phys. Chem. B **111**, 6104 (2007).

[48] S. Hyodo and K. Okabayashi, "Raman intensity study of local structure in non-aqueous electrolyte solutions. I. Cation-solvent interaction in $LiClO_4$/ethylene carbonate," Electrochim. Acta **34**, 1551 (1989).

[49] E. Cazzanelli, F. Croce, G. B. Appetecchi, F. Benevelli, and P. Mustarelli, "Li^+ solvation in ethylene carbonatepropylene carbonate concentrated solutions: A comprehensive model," J. Chem. Phys. **107**, 5740 (1997).

[50] M. Morita, Y. Asai, N. Yoshimoto, and M. Ishikawa, "A Raman spectroscopic study of organic electrolyte solutions based on binary solvent systems of ethylene carbonate with low viscosity solvents which dissolve different lithium salts," J. Chem. Soc., Faraday Trans. **94**, 3451 (1998).

[51] K. Kondo, M. Sano, A. Hiwara, T. Omi, M. Fujita, A. Kuwae, M. Iida, K. Mogi, and H. Yokoyama, "Conductivity and solvation of Li^+ ions of $LiPF_6$ in propylene carbonate solutions," J. Phys. Chem. B **104**, 5040 (2000).

[52] Y. Saito, H. Yamamoto, H. Kageyama, O. Nakamura, T. Miyoshi, and M. Matsuoka, "Investigation of the solution condition of lithium electrolyte solutions with $LiCF_3SO_3$ salt," J. Mater. Sci. **35**, 809 (2000).

[53] Z. Wang, W. Gao, X. Huang, Y. Mo, and L. Chen, "Spectroscopic studies on interactions and microstructures in propylene carbonate LiTFSI electrolytes," J. Raman Spectrosc. **32**, 900 (2001).

[54] Y. Yamada, Y. Koyama, T. Abe, and Z. Ogumi, "Correlation between charge-discharge behavior of graphite and solvation structure of the lithium ion in propylene carbonate-containing electrolytes," J. Phys. Chem. C **113**, 8948 (2009).

[55] H. L. Yeager, J. D. Fedyk, and R. J. Parker, "Spectroscopic studies of ionic solvation in propylene carbonate," J. Phys. Chem. **77**, 2407 (1973).

[56] K. Hayamizu, Y. Aihara, S. Arai, and C. G. Martinez, "Pulse-gradient spin-echo ^1H, ^7Li, and ^{19}F NMR diffusion and ionic conductivity measurements of 14 organic electrolytes containing $LiN(so_2cf_3)_2$," J. Phys. Chem. B **103**, 519 (1999).

[57] J. Barthel, R. Buchner, and E. Wismeth, "FTIR spectroscopy of ion solvation of $LiClO_4$ and LiSCN in acetonitrile, benzonitrile, and propylene carbonate," J. Solution Chem. **29**, 937 (2000).

[58] H. Tsunekawa, A. Narumi, M. Sano, A. Hiwara, M. Fujita, and H. Yokoyama, "Solvation and ion association studies of $LiBF_4$-propylenecarbonate and $LiBF_4$-propylenecarbonate-trimethyl phosphate solutions," J. Phys. Chem. B **107**, 10962 (2003).

[59] O. Borodin and G. D. Smith, "Quantum chemistry and molecular dynamics simulation study of dimethyl carbonate: Ethylene carbonate electrolytes doped with $LiPF_6$," J. Phys. Chem. B **113**, 1763 (2009).

[60] K. Leung and J. L. Budzien, "*Ab initio* molecular dynamics simulations of the initial stages of solid-electrolyte interphase formation on lithium ion battery graphitic anodes," Phys. Chem. Chem. Phys. **12**, 6583 (2010).

[61] P. Ganesh, D. Jiang, and P. R. C. Kent, "Accurate static and dynamic properties of liquid electrolytes for Li-ion batteries from *ab initio* molecular dynamics," J. Phys. Chem. B **115**, 3085 (2011).

[62] M. D. Bhatt, M. Cho, and K. Cho, "Density functional theory calculations and *ab initio* molecular dynamics simulations for diffusion of Li^+ within liquid ethylene carbonate," Model. Simul. Mater. Sci. Eng. **20**, 065004 (2012).

[63] J. P. Perdew, K. Burke, and M. Ernzerhof, "Generalized gradient approximation made simple," Phys. Rev. Lett. **77**, 3865 (1996).

[64] D. R. Hamann, M. Schlüter, and C. Chiang, "Norm-conserving pseudopotentials," Phys. Rev. Lett. **43**, 1494 (1979).

[65] L. Kleinman and D. M. Bylander, "Efficacious form for model pseudopotentials," Phys. Rev. Lett. **48**, 1425 (1982).

[66] G. B. Bachelet, D. R. Hamann, and M. Schlüter, "Pseudopotentials that work: From H to Pu," Phys. Rev. B **26**, 4199 (1982).

[67] See http://www.icmab.es/dmmis/leem/siesta/Pseudopotentials/periodictable-intro.html for Siesta pseudopotential database (based on Abinit pseudopotentials). (Accessed on 29 November 2011.)

[68] Y. Wang, S. Nakamura, M. Ue, and P. B. Balbuena, "Theoretical studies to understand surface chemistry on carbon anodes for lithium-ion batteries: Reduction mechanisms of ethylene carbonate," J. Am. Chem. Soc. **123**, 11708 (2001).

[69] B. Hess, C. Kutzner, D. van der Spoel, and E. Lindahl, "GROMACS 4: Algorithms for highly efficient, load-balanced, and scalable molecular simulation," J. Chem. Theory Comput. **4**, 435 (2008).

[70] W. L. Jorgensen, D. S. Maxwell, and J. Tirado-Rives, "Development and testing of the OPLS all-atom force field on conformational energetics and properties of organic liquids," J. Am. Chem. Soc. **118**, 11225 (1996).

[71] L. B. Silva and L. C. G. Freitas, "Structural and thermodynamic properties of liquid ethylene carbonate and propylene carbonate by Monte Carlo simulations," J. Mol. Struct.: THEOCHEM **806**, 23 (2007).

[72] G. Bussi, D. Donadio, and M. Parrinello, "Canonical sampling through velocity rescaling," J. Chem. Phys. **126**, 014101 (2007).

[73] M. Parrinello and A. Rahman, "Polymorphic transitions in single crystals: A new molecular dynamics method," J. Appl. Phys. **52**, 7182 (1981).

[74] T. Schneider and E. Stoll, "Molecular-dynamics study of a three-dimensional one-component model for distortive phase transitions," Phys. Rev. B **17**, 1302 (1978).